Environmental Science & Technology

Article

Cite This: Environ. Sci. Technol. XXXX, XXX, XXX−XXX

pubs.acs.org/est

Manganese Increases Lead Release to Drinking Water

Benjamin F. Trueman,[†] Brittany S. Gregory,[†] Nicole E. McCormick,[†] Yaohuan Gao,[†] Stephanie Gora,[†] Tim Anaviapik-Soucie,[‡,§] Vincent L'Hérault,[‡] and Graham A. Gagnon*[,†]

[†]Department of Civil & Resource Engineering, Dalhousie University, Halifax, NS CAN, B3H 4R2

[‡]ARCTIConnexion, Québec, QC CAN, G1L 1Y8

[§]Community of Pond Inlet, Pond Inlet, NU CAN, X0A 0S0

Supporting Information

ABSTRACT: Lead and manganese are regulated in drinking water due to their neurotoxicity. These elements have been reported to co-occur in drinking water systems, in accordance with the metal-scavenging properties of MnO_2. To the extent that manganese is a driver of lead release, controlling it during water treatment may reduce lead levels. We investigated transport of lead and manganese at the tap in a full-scale distribution system: consistent with a cotransport phenomenon, the two metals were detected in the same colloidal size fraction by size-exclusion chromatography with multielement detection. We also studied the effect of manganese on lead release using a model distribution system: increasing manganese from 4 to 215 $\mu g\ L^{-1}$ nearly doubled lead release. This effect was attributed primarily to deposition corrosion of lead by oxidized phases of manganese, and we used 16S rRNA sequencing to identify bacteria that may be relevant to this process. We explored the deposition corrosion mechanism by coupling pure lead with either MnO_2-coated lead or pure lead exposed to MnO_2 in suspension; we observed galvanic currents in both cases. We attributed these to reduction of Mn(IV) under anaerobic conditions, and we attributed the additional current under aerobic conditions to oxygen reduction catalyzed by MnO_2.

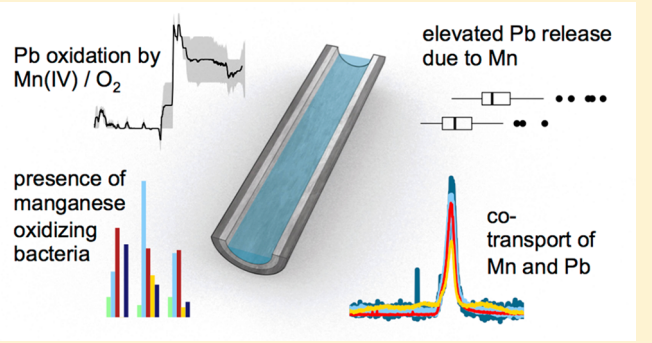

INTRODUCTION

Lead (Pb) is a neurotoxin with cognitive effects even at low exposure levels,[1] and drinking water represents an important contemporary exposure route.[2−4] Studies have linked manganese (Mn) intake via drinking water with neurotoxicity in children,[5−8] and coexposure to lead and manganese may diminish IQ interactively.[7] That is, lead toxicity could be greater among children with high manganese intake. In light of health risks, a maximum concentration of 100 $\mu g\ Mn\ L^{-1}$ has been proposed recently in Canada,[9] and a new maximum of 5 $\mu g\ Pb\ L^{-1}$ has just been adopted.[10] In the U.S., monitoring for lead and manganese is required under the Lead and Copper Rule[11] and the Fourth Unregulated Contaminant Monitoring Rule,[12] respectively.

Lead in drinking water is released primarily from system components, while manganese originates mainly from source water. Manganese has been shown to accumulate on lead,[13−15] where it is typically present in amorphous oxide deposits.[13,14] These may interfere with formation of protective lead orthophosphate[16] or lead(IV) oxide[15] films.

MnO_2 may also increase lead release, as iron oxides may,[17,18] by deposition corrosion. MnO_2 has sufficient electrical conductivity to support oxygen reduction,[19,20] and deposits on lead might provide sites for this reaction. Manganese(IV) may dissolve reductively by accepting electrons liberated in the oxidation of lead; a similar mechanism has been proposed to explain MnO_2 deposition corrosion of stainless steel.[21] These mechanisms are linked with biological oxidation of manganese: biogenic MnO_2 has been observed on corroding surfaces coated in biofilm.[21] Moreover, manganese reduced in the oxidation of lead could be reoxidized biologically.[21]

MnO_2 is an effective trace metal scavenger,[22−25] and it represents—like iron oxide[26−28]—a potential vector for lead transport.[29] Lead and MnO_2 exhibit a preferred association,[22−25] and biogenic MnO_2 may adsorb even more lead than chemically oxidized manganese. Due to its greater specific surface area, biogenic MnO_2 in one study adsorbed 2−5 times more lead than synthetic MnO_2.[30] Consistent with the reported affinity of lead for MnO_2, correlation between particulate lead and manganese has been reported in drinking water.[15] Suspended colloidal MnO_2 could serve as a mobile sink for lead released from corrosion scale, maintaining low activity of lead in solution and promoting undersaturated conditions (i.e., dissolution of the solubility-controlling phase) as described in general elsewhere.[31,32] MnO_2 deposits may

Received: January 15, 2019
Revised: March 12, 2019
Accepted: April 5, 2019
Published: April 5, 2019

DOI: 10.1021/acs.est.9b00317
Environ. Sci. Technol. XXXX, XXX, XXX−XXX

accumulate lead in a similar manner, representing a potential source of lead in drinking water.[15,27,28]

Here, we investigated manganese interactions with lead at several scales. Previously, in a full-scale system with low manganese levels (<20 μg L^{-1}), we used size-exclusion chromatography (SEC) with multielement detection to identify a strong correlation between colloidal lead and iron in tap water samples from 23 homes.[26] On the basis of standards, varying separation parameters, and supplementary filtration, we interpreted this as an indicator of colloidal particles rich in lead and iron. Here, we sought to determine whether, in a full-scale system with higher levels of manganese (>130 μg L^{-1}), a similar correlation could be observed between lead and manganese in the colloidal size range. Our data suggest that manganese, iron, and natural organic matter (NOM) all influence speciation and transport of lead from source to tap.

We also evaluated the effect of manganese on lead release in a model distribution system, and we identified known manganese-oxidizing bacteria (MOB) at the pipe surface. In additional experiments, we characterized galvanic corrosion of lead by MnO_2, showing that manganese deposition corrosion is a viable explanation for many of our observations.

MATERIALS AND METHODS

Full-Scale System. First-draw samples were collected at randomly selected times during the day at taps in two separate buildings in a full-scale water system. Details are provided in the Supporting Information. We selected a system supplied by chlorinated surface water from a river-fed reservoir, and water quality is summarized in Table S1.

Annular Reactors. We used annular reactors to simulate water distribution mains. Four reactors were operated in parallel at 50 rpm to achieve a shear stress of 0.25 N m^{-2}, modeling a flow rate of 0.3 m s^{-1} in a 100 mm diameter smooth pipe.[33] Flow rates were maintained to achieve a retention time of 2 h and polycarbonate coupons were mounted within the reactors as inert surfaces for biofilm growth.[34,35] Before the experiment, annular reactors and coupons were cleaned and sterilized according to procedures detailed elsewhere.[36−38]

Tap water—dechlorinated by granular activated carbon—was used as the feedwater to the annular reactors. Activated carbon filtration may have influenced the model system microbiome,[39] but this effect would have been constant across experimental treatments. Here, the dechlorinated condition is representative of water systems that either do not maintain[40] or have difficulty maintaining[41] a disinfectant residual. The full-scale system we studied falls into the latter category, with free chlorine residuals below 0.2 mg L^{-1} at the tap (Table S1). Alkalinity in reactor feedwater was 19.5 mg $CaCO_3$ L^{-1}, and dissolved oxygen was at or near saturation (approximately 9 mg L^{-1} at 20 °C, see the feedwater summary, Table S2). During stagnation in lead pipes, dissolved oxygen was expected to deplete according to empirical curves published elsewhere.[42]

Feedwater was modified to achieve the experimental conditions. Two reactors were operated at the ambient feedwater concentration (median 4.0 μg L^{-1}), and two were dosed with $MnSO_4$ to yield a median effluent concentration of 215 μg Mn L^{-1}. This exceeds guidelines[9] but is comparable with levels in the full-scale system (135−191 μg Mn L^{-1}). To assess the effect of nutrients on biofilm, two effluent orthophosphate concentrations— median 1.01 and 1.31 mg PO_4 L^{-1}—were investigated as a two-factor orthogonal design. That is, all four combinations of two orthophosphate and two manganese concentrations were represented. The median difference between orthophosphate doses was 0.54 with an interquartile range of 0.04−0.71 mg PO_4 L^{-1}.

Before introducing lead pipes to the system, reactors were operated over a 12-week period at nominal doses of 1.7 and 2.2 mg PO_4 L^{-1}, achieved with additional H_3PO_4. Following this, the low orthophosphate dose (1.01 mg L^{-1}) was obtained by passing feedwater through $Fe(OH)_3$ filters, and the high dose (1.31 mg L^{-1}) represented the ambient feedwater concentration (zinc orthophosphate was added at the treatment plant). Median iron in filter effluent was low, 9.3 μg L^{-1} (n = 12), but total organic carbon (TOC) was greater in annular reactor effluent by 0.6 mg L^{-1} at the higher orthophosphate dose (1.8 vs 1.2 mg TOC L^{-1}). That is, $Fe(OH)_3$ filters also removed TOC. This difference may have influenced biofilm, but the effect was not separable from the effect of orthophosphate (i.e., TOC and orthophosphate were positively correlated). To the extent that higher TOC increased lead release, we underestimated the effect of orthophosphate. However, differences in TOC were probably not a strong determinant of lead solubility: previously, we found little evidence of Pb−NOM complexation in distributed water from the same source.[43] This was likely due to removal of metal-complexing organic fractions by coagulation at the treatment plant. Median annular reactor effluent temperature and pH were 21 °C and 7.25 (after chemical addition), respectively. Owing to minor contamination from a previous experiment, annular reactors released detectable levels of lead (median 17 μg L^{-1}), but they were typically less than 0.5% of pipe effluent concentrations.

Lead Pipe Sections. Effluent from each annular reactor was fed directly into a lead pipe section; each manganese concentration was represented by two sections. Before the experiment, corrosion scale was removed from the recovered pipe sections by dissolution in 1.8 M HNO_3. Hydrocerussite and hydroxypyromorphite have been identified previously as the only crystalline phases in lead pipe scale extracted from the same distribution system,[43] and both are soluble in dilute HNO_3.[44] Pipe sections were acclimated over a 16-week period under the experimental conditions; the duration of conditioning was chosen based on previous studies.[45,46] After conditioning, 6 h stagnant, unfiltered water samples were collected weekly (Figure S1) in HNO_3-washed 0.5 L HDPE bottles, preserved with trace metal-grade HNO_3, and digested at 105 °C with additional HNO_3 (*Standard Method 3030 E*).[47] Otherwise, flow through the system was approximately 8 mL min^{-1}.

Galvanic Corrosion Cells. We conducted separate experiments in a single-chamber galvanic cell (Figure S2), logging current with a multimeter (±1.2% accuracy in the relevant current range). The cell contained two lead coupons (approximately 40 × 10 × 2 mm^3), one with and one without a deposited layer of MnO_2. Coupons were cut from a sheet (Canada Metal) and submerged 30 mm in 60 mg L^{-1} $NaHCO_3$ solution (pH 8.4). Freshly prepared solution was saturated with respect to dissolved oxygen, and the deaerated condition was achieved by nitrogen sparging for 0.5 h[48] with a pH change of less than 0.2. Before each experiment, scale was removed from all pure lead anodes by immersion in 1.8 M HNO_3 (lead does not passivate in dilute HNO_3).[49] At the end of each experiment, the electrode assembly was removed from

DOI: 10.1021/acs.est.9b00317
Environ. Sci. Technol. XXXX, XXX, XXX−XXX

the glass cell, the electrolyte was acidified to pH < 2 with 0.2 mL of trace metal-grade HNO_3, and the solution was held for 24 h to dissolve particulate and adsorbed lead. Tests were run 3−4 times.

MnO_2 was deposited anodically onto one of the two lead electrodes in a separate bath of 1.0 M $MnSO_4{\cdot}H_2O$, as described elsewhere (half-reactions are summarized in Table S3).[50] A potential difference of approximately 8 V was maintained over 5 h between the lead electrode and a graphite counter electrode. After deposition, the MnO_2-coated lead electrode was removed from the $MnSO_4$ solution and washed with ultrapure water. Some PbO_2 formation was expected during electrodeposition, but none was detected by X-ray diffraction (XRD) or X-ray photoelectron spectroscopy (XPS) (see *Galvanic corrosion of lead by MnO_2*). This was probably due to reductive dissolution of PbO_2 by Mn(II).[51,52] XRD analysis of the deposited layer after removal from the surface did indicate some α-PbO formation (Figure S3) that was not detected by in situ analysis of the film; α-PbO likely formed below the X-ray penetration depth at the interface with lead.

We also investigated corrosion of lead by suspended MnO_2 in a two-chamber lead−lead galvanic cell (Figure S4) with an anion-exchange membrane separating the chambers. Each lead coupon (75 × 12 × 1.5 mm^3, Cosasco) was cleaned sequentially with acetone, ethanol, and dilute HNO_3 before tests. The bottom 50 mm of each coupon was submerged in 200 mL of 60 mg L^{-1} $NaHCO_3$, deaerated as in the oxygen-free single-cell experiments. In both experiments, the deaerated condition represents the limiting case of near-complete oxygen depletion over long stagnation periods within lead pipes or premises plumbing.[42]

MnO_2 was synthesized by thermal decomposition of $Mn(NO_3)_2{\cdot}xH_2O$ at 310 °C. A mortar and pestle was used to grind the MnO_2 into a fine powder, and the particle size in suspension was estimated at 442 ± 34 nm by dynamic light scattering (Malvern Zetasizer). After deaerating both half-cells, equilibrium current was collected for 1 h and then 60 mg of MnO_2 was added to one of the two chambers. Conditions in the two chambers were otherwise identical. The chamber dosed with MnO_2 was deaerated again before reconnection, and current in the presence of MnO_2 was measured for another hour. Tests were run in duplicate.

Other Analytical Methods. Data analysis, the MOB enumeration method, sequencing methods, XRD, XPS, and SEC are all described in the Supporting Information and elsewhere.[26,53]

RESULTS AND DISCUSSION

Lead and Manganese Cotransport in a Full-Scale Water System. Size-fractionation of water samples collected in the full-scale system was consistent with cotransport of manganese, iron, and lead in the colloidal size range (Figure 1a). These elements eluted together at high apparent molecular weight (8.6 mL peak retention volume) in samples representing two water taps in separate buildings. Nominally, colloidal particles were sized between 17 nm (the hydrodynamic diameter of thyroglobulin) and 450 nm (the pore size at which samples were filtered). Negative peaks at retention volumes of 20−25 mL were due to equilibrium disturbances associated with the sample solvent—which differed in composition from the mobile phase—passing through the column. These have been observed in previous studies.[54,55]

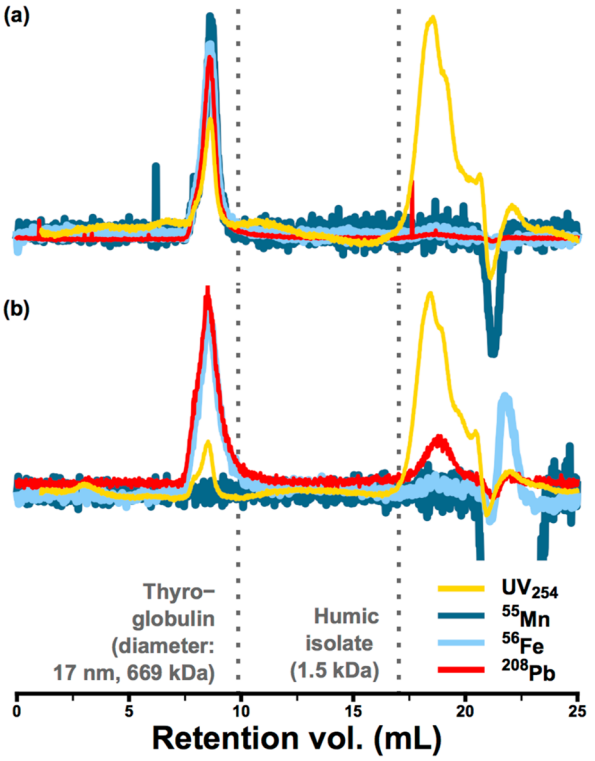

Figure 1. (a) Size-exclusion chromatograms, representing one of two tap water samples (first round), were consistent with cotransport of manganese, lead, and iron as colloidal particles, possibly stabilized by NOM. (b) Size-exclusion chromatograms, representing one of two tap water samples (second round), were consistent with cotransport of lead and iron as colloidal particles; manganese was not detected in the high apparent molecular weight fraction. Lead was also present at low apparent molecular weight, coincident with the principal UV_{254} peak representing NOM. This signal was interpreted as a Pb−NOM complex. In both panels, the ordinate is represented in arbitrary units; scales differ by analyte. Peak retention volumes for lead, manganese, and iron were almost identical for the two samples at each round, but for brevity, only one is represented here.

At the initial sampling round, size separation provided no evidence of Pb−NOM complexation: lead was detected only at high molecular weight (Figure 1a). This is consistent with preferential partitioning of lead to iron-rich colloidal particles as observed in other surface waters.[56] Evidence of colloidal metals transport is also consistent with expectations based on water quality: the combination of low ionic strength and high organic carbon would be expected to promote formation of stable colloidal metal oxide particles with surfaces coated in adsorbed NOM.[57−59] High molecular weight and largely hydrophobic[60] NOM adsorbs preferentially to iron oxides,[59,61] and specific UV absorbance predicts a hydrophobic acid fraction of approximately 0.5 for this water, based on a reported correlation (r = 0.95) for 30 U.S. rivers.[62]

At the second sampling round, manganese was not detected in a colloidal fraction. Soluble manganese was likely retained on the stationary phase, as lead and iron are; this would explain why it was not detected during separation. Lead did elute at low apparent molecular weight (18.7 mL peak retention volume), coincident with the principal UV_{254} peak representing aromatic NOM (Figure 1b) (aliphatic compounds absorb poorly at 254 nm but may also be important in this context). In contrast to data from the first round, this is consistent with

DOI: 10.1021/acs.est.9b00317
Environ. Sci. Technol. XXXX, XXX, XXX−XXX

Pb−NOM complexation, as has been observed previously via SEC with UV and multielement detection.[18,63] On the basis of the elution volume of the model humic isolate, the molecular weight of the Pb−NOM complex was estimated at less than 1.5 kDa. Differences in the speciation of lead between the two sampling rounds remain unexplained, but variation in water age, stagnation time, concentrations of other metals, and free chlorine concentration may have been important factors in these observations.

Effect of Manganese in a Model Distribution System. We also explored the effect of manganese on lead release experimentally, using annular reactors as models for distribution mains and lead pipe sections to represent legacy lead service lines. Elevated manganese accompanied greater lead release in the model system, as estimated by an additive linear model: compared with lead release at the background manganese concentration, release from pipe sections was greater by 8.0 mg Pb L^{-1} (95% CI: 4.0−12.0 mg L^{-1}, p = 0.025, n = 53 per group) at the high manganese concentration (215 μg L^{-1}, Figure 2b). Mean effluent lead concentrations at the high and low manganese levels were 17.2 and 9.2 mg L^{-1}, respectively. Most of this lead was particulate: solubility under the conditions in the model system has been predicted at approximately 25 μg Pb L^{-1}.[67] The dominance of particulate lead accords with the correlation between turbidity and lead release: as a linear predictor, lead concentrations explained R^2 = 74% of the variation in effluent turbidity (Figure S5, n = 254).

Orthophosphate was also a significant determinant of lead release as estimated by the additive model: lead in pipe effluent was lower by 4.0 mg L^{-1} (95% CI: 0.1−8.0 mg L^{-1}, p = 0.049, n = 53 per group) at the higher orthophosphate dose (1.31 mg PO_4 L^{-1}). Mean effluent lead concentrations at the high and low orthophosphate doses were 11.1 and 15.1 mg L^{-1}, respectively. In general, orthophosphate reduces lead solubility by promoting formation of relatively insoluble minerals: hydroxypyromorphite and chloropyromorphite are two possibilities that have been identified in field-extracted lead corrosion scale.[45,64] Orthophosphate also reduces particulate lead release,[65] but excess orthophosphate may promote formation of stable colloidal lead.[66] Given the water quality, pyromorphite (hydroxyl- or chloro-) and a mixture of lead carbonates—including cerussite and hyrdrocerussite—were expected as the dominant phases within lead pipes in the model system.[67] Lead(IV) oxide was not expected due to the low free chlorine residual and the presence of orthophosphate, which inhibits PbO_2 formation.[68] In addition to its impact on scale composition, orthophosphate may also be an important determinant of microbial community structure within distribution system biofilms (see *Presence of manganese oxidizing bacteria*).

Possible Mechanisms for the Effect of Manganese. Given the increase in manganese of 0.2 mg L^{-1}, the accompanying increase in lead (8.0 mg L^{-1}) cannot be explained by adsorption to MnO_2 alone. Several other possibilities exist: perhaps most importantly, deposits of MnO_2 may have supported oxygen reduction[19] at the pipe surface, accelerating oxidation and release of lead. Manganese(IV) itself may have acted as an acceptor for electrons liberated in the oxidation of lead. MOB colonization has been recognized as a potential factor in the pitting corrosion of stainless steel,[21] and manganese(IV) reduced by lead could be redeposited within lead pipes via biological oxidation.[21]

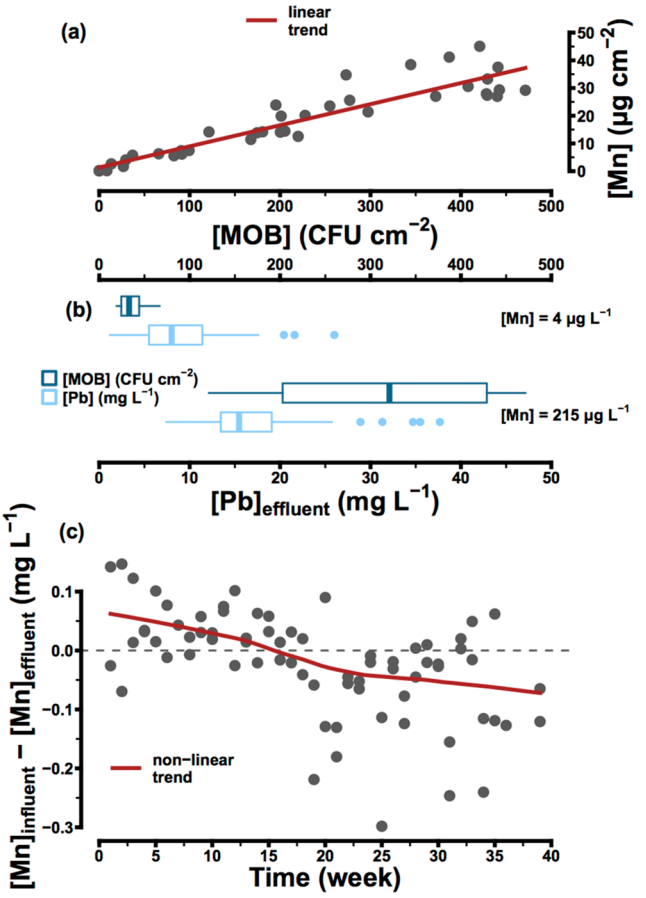

Figure 2. (a) Surface concentrations of Mn and MOB were highly correlated over time at the high influent manganese concentration (r = 0.95). (b) Lead in pipe effluent and MOB in annular reactors were greater by 8.0 mg Pb L^{-1} and 290 CFU cm^{-2} at the high influent manganese concentration (215 μg L^{-1}, n = 2 pipes/reactors) compared with the low concentration (4 μg L^{-1}, n = 2 pipes/reactors). Boxes enclose the interquartile range, bold vertical lines divide the boxes at the median, and whiskers extend to the most extreme value within 1.5 times the interquartile range; points beyond these limits are displayed individually. (c) At 215 μg L^{-1} influent manganese, a net accumulation within lead pipes was observed over weeks 1−15 of the experiment; a net release was observed from week 16 on. The time trend (conditional mean) was estimated by robust local linear regression (red line). (N.B., parts c and a include 10−12 weeks of data from the conditioning period.)

Several observations suggest that MOB facilitated deposition of manganese within annular reactors. Moreover, the presence of a pre-established, lead-tolerant, manganese-oxidizing biofilm upstream from the lead pipes may have aided their colonization with MOB (see *Presence of manganese oxidizing bacteria*). Upstream from the lead pipes, polycarbonate coupons in annular reactors with added manganese had median 26.3 μg Mn cm^{-2} (interquartile range: 14.4−29.6 μg Mn cm^{-2}, n = 24) and 321 CFU cm^{-2} (204−428 CFU cm^{-2}) of MOB (Figure 2b). Coupons in the annular reactors at the background manganese concentration had much less of both: 1.74 μg Mn cm^{-2} (1.09−2.10 μg Mn cm^{-2}) and 33.0 CFU cm^{-2} (24.5−44.1 CFU cm^{-2}). Surface concentrations of manganese and MOB were also highly correlated over time (r = 0.95, Figure 2a, n = 48).

Consistent with a deposition mechanism, manganese was nonconservative across the length of lead pipe: manganese

DOI: 10.1021/acs.est.9b00317
Environ. Sci. Technol. XXXX, XXX, XXX−XXX

accumulation within pipe sections was inferred over time at the high influent concentration (215 μg Mn L^{-1}) as the difference between influent and effluent manganese (Figure 2c, n = 72). An apparent accumulation was observed from weeks 1−15 and, by extrapolation, over the conditioning period as well. This was interpreted as deposition at the lead surface due to MOB. A net release was observed from week 16 on; this may be explained by reductive Mn(IV) dissolution, by lead or by manganese-reducing bacteria.[21,69] Release of manganese-rich particles from corrosion scale or, given the particle-rich environment, partitioning of Mn(II) to suspended solids are also possible explanations: both manganese and lead were statistically significant predictors of turbidity in pipe effluent (see Supporting Information). Previous work suggests that the speciation of manganese in surface waters is complex, with dissolved, organically complexed, colloidal, and larger particulate fractions.[70]

Galvanic Corrosion of Lead by MnO_2. We explained elevated lead release in the manganese-enriched model system with reference to MnO_2 deposition via biological Mn(II) oxidation. We explored this idea in follow-up experiments where MnO_2 was either electrochemically deposited on lead or suspended in an electrolyte that contacted lead.

Deposition of MnO_2 on lead generated significant galvanic current, as determined by coupling the coated electrode with a pure lead electrode (Figure 3b,c). Even after 16 h, currents ranged from 11−37 μA (n = 7 runs), corresponding to theoretical release rates of 426−1432 μg Pb L^{-1} h^{-1}. The drop in current over time was attributed largely to scale formation, which was visible in all experiments. Moreover, observed lead was 28−79% of that predicted by current, and the difference can be accounted for by scale. Despite scaling, we showed in previous work that galvanic current due to coupling of lead and pure Fe_3O_4 remained above 2 μA (77 μg Pb L^{-1} h^{-1}) for at least several weeks with regular water changes.[18]

Galvanic current in the deaerated system (Figure 3b) was attributed primarily to reduction of Mn(IV) at the cathode and oxidation of lead at the anode. This was in accordance with the surface characterization: the newly deposited film was identified by XRD as poorly crystalline akhtenskite (ε-MnO_2, Figure 3a, t = 0 h). The predominant oxidation state of manganese at the coupon surface was +4, as determined by XPS based on the binding energy of the $2p_{3/2}$ peak (642.5 eV, Figure 4a)[71] and the magnitude of 3s multiplet splitting (4.3 eV, Figure 4b).[72] In transition metals, multiplet splitting is caused by exchange coupling between the 3s hole and 3d electrons; the energy difference between peaks can be used to distinguish between the II, III, and IV oxidation states of manganese.[73]

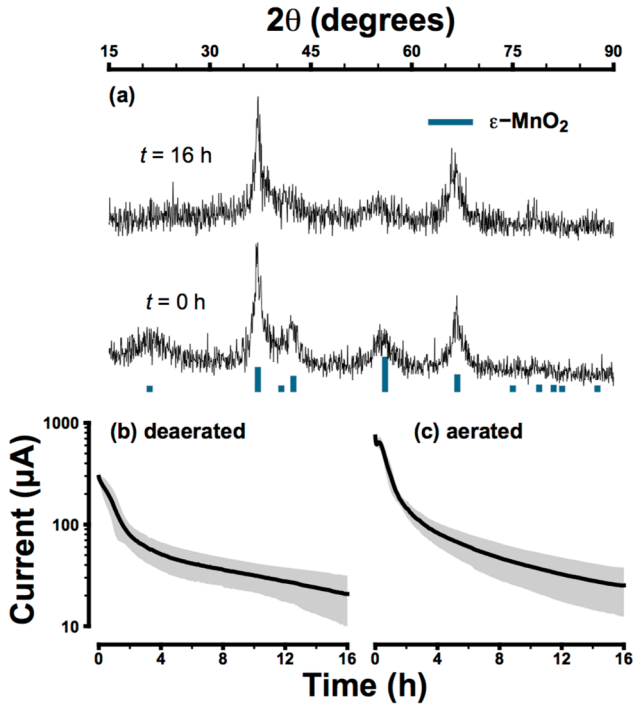

Figure 3. (a) XRD patterns representing MnO_2 deposited on lead. Reflections at t = 0 h were attributed to poorly crystalline akhtenskite (ε-MnO_2), which exhibited diminished crystallinity after reaction with metallic lead (t = 16 h). The ordinate is represented in arbitrary units. (b) Galvanic current due to coupling of lead (anode) with MnO_2-coated lead (cathode) in a deaerated bicarbonate solution. (c) Galvanic current due to the same coupling in an aerated bicarbonate solution. Black lines represent the mean of (at least) triplicate experiments and shaded regions represent ±1 standard deviation about the mean.

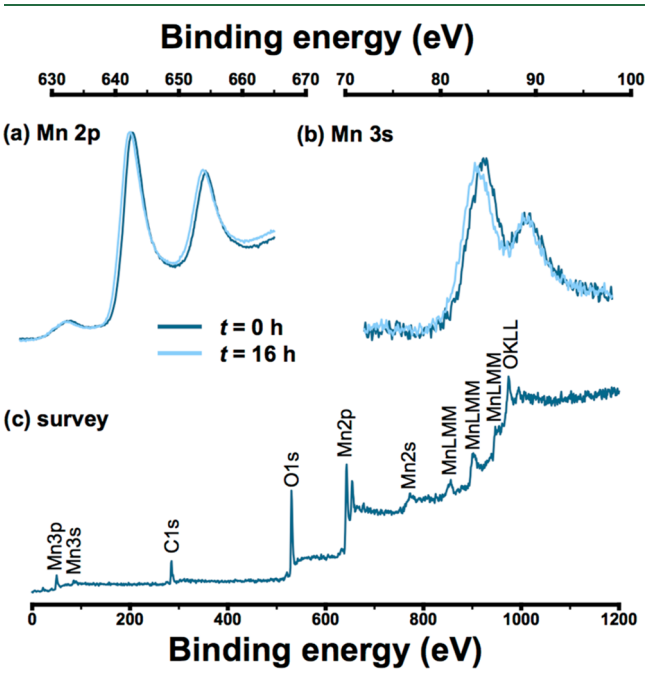

Figure 4. The predominant manganese oxidation state was determined by XPS to be +4 at t = 0 h, based on (a) the binding energy of the $2p_{3/2}$ peak (642.5 eV) and (b) the magnitude of 3s multiplet splitting (4.3 eV). A full XPS peak survey is provided (c) as a visual summary of elemental composition. Even in the aerated system, shifts in the positions of the $2p_{3/2}$ peak (642.4 eV) and an increase in the magnitude of 3s multiplet splitting (5.0 eV) were consistent with some reduction of Mn(IV) by reaction with metallic lead (t = 16 h).

Manganese release in the deaerated system was highly variable (median: 22 μg L^{-1}, range: 10−610 μg L^{-1}). To some extent, this release may represent spalling of the MnO_2 film, but observed manganese in the water phase represented just 2% of that predicted from current by Faraday's law. Although other reactions cannot be ruled out, this suggests formation of a reduced manganese phase on the cathode surface (e.g.,

DOI: 10.1021/acs.est.9b00317
Environ. Sci. Technol. XXXX, XXX, XXX−XXX

MnOOH)[21] or adsorption of Mn^{2+} within the system[74] or both.

Additional galvanic current in the aerated system (Figure 3c) may have been due to reduction of dissolved oxygen at the MnO_2–water interface. Total charge transfer was greater by 2.17 C, on average, in the aerated compared with the deaerated system, and higher currents were attributed to this half-reaction. Furthermore, efficient oxygen reduction at MnO_2 surfaces has been reported elsewhere.[19,20] Still, a shift in the position of the $2p_{3/2}$ XPS peak to slightly lower binding energy (642.4 eV) and an increase in the magnitude of 3s multiplet splitting to 5.0 eV were consistent with some reduction of Mn(IV) at the surface even in the aerated system (Figure 4a,b). The experimental XRD trace at t = 16 h also exhibited decreased crystallinity, consistent with phase changes at the MnO_2 surface over the reaction period (Figure 3a).

Manganese release under aerated conditions was also highly variable (median: 836 $\mu g\ L^{-1}$, range: 37–14110 $\mu g\ L^{-1}$). Again, this variability may have been amplified due to release of particulate manganese from the MnO_2 film. Over both conditions (aerated and deaerated), observed manganese was uncorrelated with the time-integrated current signal (Pearson correlation: −0.06, p = 0.90). Conversely, charge transfer as a linear predictor explained R^2 = 67% of the variation in lead release (Figure S6).

Corrosion of lead also occurred when particulate MnO_2 contacted lead in suspension, as determined in a separate lead–lead galvanic corrosion experiment. Figure 5 shows

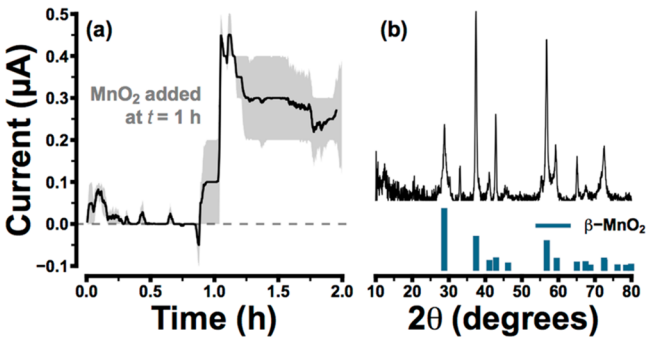

Figure 5. (a) Addition of MnO_2 to one-half-cell at t = 1 h resulted in oxidation of lead in the other, as indicated by an increase in the magnitude of galvanic current between the two lead electrodes. The black line denotes the mean and the shaded region spans the range of duplicate tests; the current signal was smoothed with a 200-point moving average. (Raw data with computed detection limits are provided in Figure S7.) (b) MnO_2 was identified as pyrolusite (β-MnO_2) by XRD.

equilibrium current (t = 0 to 1 h) resulting from coupling two pure lead electrodes in separate chambers divided by an anion-exchange membrane. Addition of MnO_2 to one of the two chambers caused oxidation of lead in the other chamber, as indicated by the increase in galvanic current at t = 1 h (i.e., flow of electrons to the MnO_2-exposed electrode). Here, the function of the membrane was to allow current flow through the electrolyte while ensuring that MnO_2 contacted just one electrode.

Given the anaerobic condition, measured current was attributed to reductive dissolution of Mn(IV) at the lead–water interface. At t = 2 h, manganese in 0.22 μm filtrate was 990 $\mu g\ L^{-1}$ on average, but charge transfer predicted release of just 1.5 $\mu g\ Mn^{2+}\ L^{-1}$, corresponding to 5.5 $\mu g\ Pb^{2+}\ L^{-1}$ per hour. Excess soluble manganese was due to (1) dissolution or colloidal dispersion of β-MnO_2 independent of lead oxidation in the other chamber and (2) localized oxidation of lead by MnO_2. The latter is consistent with the presence of pits in MnO_2-exposed lead surface. This reaction would not have been reflected in measured current, but it may have contributed significantly to reductive dissolution of MnO_2.

Presence of Manganese Oxidizing Bacteria. Given our hypothesis that biological manganese oxidation accelerated lead corrosion, we analyzed microbial communities within annular reactors and lead pipes (1) to identify known MOB that may have contributed to manganese deposition and (2) to determine how manganese and nutrient (C and P) availability influenced community structure.

Differences in manganese and nutrients were indeed associated with shifts in the microbial community structure within pipes and their corresponding annular reactors upstream. These changes—quantified by weighted and unweighted UniFrac dissimilarities—are represented in the space spanned by the first two principal coordinate axes in Figure 6a,b. Principal coordinate analysis clearly separated

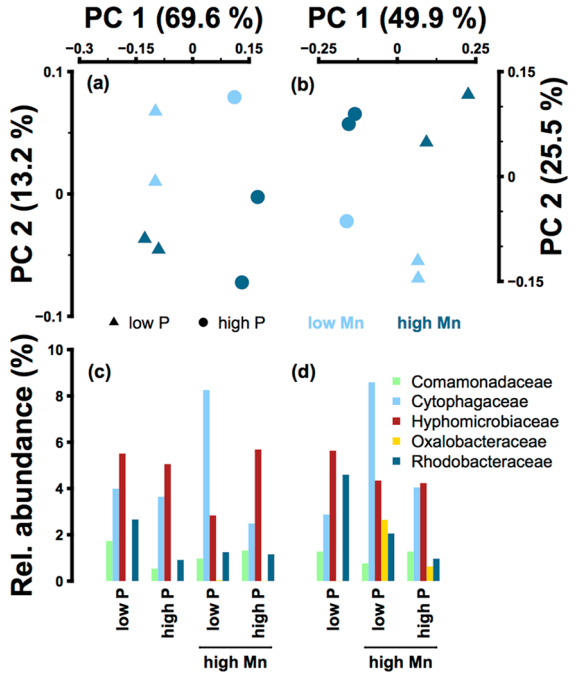

Figure 6. Represented in the space spanned by the first two principal coordinates, the unweighted (a) and weighted (b) UniFrac dissimilarities exhibited clear separation of microbial communities according to manganese and orthophosphate concentration. The variation accounted for by each principal coordinate axis is given in the axis title; plotting characters represent differences in P (and C) concentrations, and colors represent differences in Mn concentrations. Sequences matching known manganese oxidizers at the family level (unknown or matching genus) were observed in all annular reactor (c) and pipe (d) samples.

communities according to manganese and nutrient concentration but not according to reactor type (annular vs pipe). Microbial communities exposed to the high orthophosphate dose—and the accompanying high TOC concentration—were also significantly different from those exposed to the low dose (analysis of similarities, ANOSIM, on the ranked dissimilarity

DOI: 10.1021/acs.est.9b00317
Environ. Sci. Technol. XXXX, XXX, XXX–XXX

matrix, weighted, $p = 0.025$ and unweighted, $p = 0.04$, $n = 7$ experimental units). Richness (observed and estimated), Shannon diversity, and Simpson evenness indices all decreased with increasing orthophosphate dose (Table S4), consistent with previous work showing a negative correlation between species diversity and nutrient availability.[75−77] Simpson evenness was also notably low, indicating dominance by a small fraction of the total species count. Despite separation on the second principal coordinate axis, microbial communities exposed to the high manganese dose did not exhibit a statistically significant difference from those exposed to the low dose based on ANOSIM.

Sequences matching known MOB at the family level (unknown or matching genus) were observed in samples from both annular reactors and lead pipes: Comamonadaceae,[78] Cytophagaceae,[79] Hyphomicrobiaceae,[78] Oxalobacteraceae,[80] and Rhodobacteraceae (Figure 6c).[81] These data accord with the strong correlation between manganese and MOB in annular reactor biofilm. Given the similarities in community structure between pipes and annular reactors, a biofilm similarly rich in manganese and MOB may have established itself on pipe surfaces. More generally, relative abundance was dominated by the phyla Proteobacteria (35−47%), Bacteriodetes (15−36%), and Acidobacteria (8−14%). The Actinobacteria (2−11%), Nitrospirae (<1−3%), Planctomycetes (<1−14%), and Verrucomicrobia (<1−7%) were less abundant.

Families identified here that include MOB have also exhibited lead tolerance or have been found at or near corroding lead surfaces. Notably, the manganese-oxidizing Oxalobacteraceae were present in lead pipe samples at the high manganese dose and effectively absent everywhere else; members of this family have been detected previously in lead pipe corrosion scale.[82] *Cupriavidus gilardii*—of the family Oxalobacteraceae—was identified almost exclusively on lead corrosion scale at the high manganese/low orthophosphate condition (i.e., at the highest lead levels). The genome of a related species—*C. metallidurans*—contains an operon conferring lead resistance.[83] While *C. gilardii* lacks one of the genes in this operon (pbrD,[84] involved in binding Pb^{2+}) the species has a higher minimum inhibitory concentration for lead (4 mM)[84] than *C. metallidurans* (1 mM).[85] The *C. gilardii* genome does not contain homologues for MnxG, MofA, MoxA, CotA, CueO—proteins that oxidize manganese—but it does encode MntH, a protein that transports manganese into the cell.[86] High lead tolerance and manganese-transporting ability may explain the abundance of *C. gilardii* under conditions of high lead and manganese.

The families Cytophagaceae and Hyphomicrobiaceae also include species linked with lead corrosion,[87] and Cytophagaceae have been found in lead-contaminated soil[88] and mine water environments.[89] Like the Oxalobacteraceae, Cytophagaceae were detected at greatest abundance (8.6%) under conditions generating the highest lead and manganese levels in our study (i.e., at low C and P). While Comamonadaceae and Rhodobacteraceae have not been identified in lead corrosion studies to our knowledge, Comamonadaceae do exhibit lead tolerance[90] and Rhodobacteraceae have been identified in microbial mats that sequester high levels of manganese and lead.[89] The families Chitinophagaceae, Methylobacteriaceae, Sphingomonadaceae, Bradyrhizobiaceae, Enterobacteriaceae, Rhodospirillaceae were also identified within lead pipes (this study) and have been identified previously in lead corrosion studies[82,87] or have been shown to exhibit lead tolerance.[90,91] Although these families do not include known MOB, Rhodospirillaceae have been found in high manganese environments and may be involved in geochemical cycling of iron, manganese, and sulfur.[92] Like the Cytophagaceae, Rhodospirillaceae were most abundant in annular reactors (32.2%) and lead pipes (13.6%) under conditions of high manganese and low nutrients (C and P). A full list of taxa is provided as Table S5.

Environmental Implications. The primary implication of this study stems from the observation that manganese increased lead release in the model system. This was attributed mainly to oxidation of lead by oxygen on MnO_2 deposits or by Mn(IV) itself; transport of lead by manganese-rich colloidal particles played at most a minor role but may be important in other systems. To the extent that these mechanisms operate in a full-scale system, removing manganese during treatment could offer indirect benefits in terms of diminished lead release. Indeed, recent practical experience suggests that manganese removal represents a viable lead-reduction strategy.[15] This is in addition to the direct benefits associated with minimizing health effects due to manganese exposure.

Full-scale system data highlight the possibility that both manganese and NOM influence lead speciation at and transport to the tap. These data corroborate a previously reported correlation between lead and manganese,[15] and they support theoretical and experimental work[18,93] highlighting the probable complexation of lead by NOM in systems distributing unfiltered or otherwise NOM-rich water. That is, NOM may increase lead solubility under some circumstances. The complex speciation of lead in 0.45 μm filtrate highlights the need for methods to quantify the organically complexed and primarily inorganic colloidal fractions of lead and other metals.

Biofilm may also be an important determinant of lead release in drinking water systems. Preliminary work supports this notion,[94] and the MOB identified on lead in our study may have played a role in manganese-induced lead release. Manganese-reducing bacteria have been found alongside MOB,[69] and they may also be relevant to corrosion processes.[21] While our model system mirrored the low chlorine residual in the full-scale system (<0.2 mg Cl_2 L^{-1})—and chlorine depletion would be expected in lead pipes due to corrosion reactions[95]—MOB have been identified in pipe surface biofilm at higher free chlorine concentrations as well.[69]

■ ASSOCIATED CONTENT

Ⓢ Supporting Information

The Supporting Information is available free of charge on the ACS Publications website at DOI: 10.1021/acs.est.9b00317.

Water quality characterizing the model and full-scale systems, electrodeposition reactions, diversity metrics for microbial communities, alpha rarefaction curves, diagrams of experimental apparatus, identified taxa, a description of the data analysis, and additional experimental data (sequencing data are available from the NCBI Sequence Read Archive, SRA accession PRJNA514325) (PDF)

■ AUTHOR INFORMATION

Corresponding Author

*E-mail: graham.gagnon@dal.ca. Phone: 902.494.3268. Fax: 902.494.3108.

DOI: 10.1021/acs.est.9b00317
Environ. Sci. Technol. XXXX, XXX, XXX−XXX

ORCID

Benjamin F. Trueman: 0000-0002-1539-3092

Notes

The authors declare no competing financial interest.

■ ACKNOWLEDGMENTS

This work was funded by NSERC (Grant No. IRCPJ: 349838-16), Iriving Shipbuilding, and the Nunavut Research Institute. We are grateful for the technical support provided by Heather Daurie, Yuri Park, and Kelly Cameron.

■ REFERENCES

(1) Evens, A.; Hryhorczuk, D.; Lanphear, B. P.; Rankin, K. M.; Lewis, D. A.; Forst, L.; Rosenberg, D. The impact of low-level lead toxicity on school performance among children in the Chicago Public Schools: a population-based retrospective cohort study. *Environ. Health* **2015**, *14* (1), 1−9.

(2) Edwards, M.; Triantafyllidou, S.; Best, D. Elevated blood lead in young children due to lead-contaminated drinking water: Washington, DC, 2001− 2004. *Environ. Sci. Technol.* **2009**, *43* (5), 1618−1623.

(3) Zahran, S.; McElmurry, S. P.; Sadler, R. C. Four phases of the Flint water crisis: Evidence from blood lead levels in children. *Environ. Res.* **2017**, *157*, 160−172.

(4) Ng, D. Q.; Liu, S. W.; Lin, Y. P. Lead as a legendary pollutant with emerging concern: Survey of lead in tap water in an old campus building using four sampling methods. *Sci. Total Environ.* **2018**, *636*, 1510−1516.

(5) Bhang, S. Y.; Cho, S. C.; Kim, J. W.; Hong, Y. C.; Shin, M. S.; Yoo, H.; Kim, B. N. Relationship between blood manganese levels and children's attention, cognition, behavior, and academic performance—A nationwide cross-sectional study. *Environ. Res.* **2013**, *126*, 9−16.

(6) Bouchard, M.; Sauvé, S.; Barbeau, B.; Legrand, M.; Brodeur, M. E.; Bouffard, T.; Mergler, D. Intellectual impairment in school-age children exposed to manganese from drinking water. *Environ. Health Perspect.* **2011**, *119* (1), 138−143.

(7) Henn, B.; Schnaas, L.; Ettinger, A.; Schwartz, J.; Lamadrid-Figueroa, H.; Hernández-Avila, M.; Téllez-Rojo, M. Associations of early childhood manganese and lead coexposure with neurodevelopment. *Environ. Health Perspect.* **2012**, *120* (1), 126−131.

(8) Kim, Y.; Kim, B. N.; Hong, Y. C.; Shin, M. S.; Yoo, H. J.; Kim, J. W.; Cho, S. C. Co-exposure to environmental lead and manganese affects the intelligence of school-aged children. *NeuroToxicology* **2009**, *30*, 564−571.

(9) *Manganese in drinking water*; Health Canada: Ottawa, Canada, 2016; https://www.canada.ca/en/health-canada/programs/consultation-manganese-drinking-water/manganese-drinking-water.html.

(10) *Guidelines for Canadian Drinking Water Quality: Guideline Technical Document − Lead*; Health Canada: Ottawa, Canada, 2019; https://www.canada.ca/en/health-canada/services/publications/healthy-living/guidelines-canadian-drinking-water-quality-guideline-technical-document-lead.html.

(11) Maximum contaminant level goals and national primary drinking water regulations for lead and copper; *Final rule Fed. Regist.*, **1991**, *56*, 26460.

(12) Revisions to the unregulated contaminant monitoring Rule (UCMR 4) for public water systems and announcement of a public meeting; U.S. Environmental Protection Agency; *Fed. Regist.*, **2016**, *81* 92666−92692.

(13) Gerke, T.; Little, B.; Maynard, J. Manganese deposition in drinking water distribution systems. *Sci. Total Environ.* **2016**, *541*, 184−193.

(14) Schock, M.; Hyland, R.; Welch, M. Occurence of contaminant accumulation in lead pipe scales from domestic drinking-water distribution systems. *Environ. Sci. Technol.* **2008**, *42* (12), 4285−4291.

(15) Schock, M.; Cantor, A.; Triantafyllidou, S.; Desantis, M.; Scheckel, K. Importance of pipe deposits to Lead and Copper Rule compliance. *J. - Am. Water Works Assoc.* **2014**, *106* (7), E336−E349.

(16) Schock, M. Lead corrosion control 101: a journey in rediscovery. In *2017 AWWA International Symposium on Inorganics*. Detroit, MI, March 21−22, 2017.

(17) Trueman, B. F.; Gagnon, G. A. Understanding the role of particulate iron in lead release to drinking water. *Environ. Sci. Technol.* **2016**, *50* (17), 9053−9060.

(18) Trueman, B. F.; Sweet, G. A.; Harding, M. D.; Estabrook, H.; Bishop, D. P.; Gagnon, G. A. Galvanic corrosion of lead by iron (oxyhydr)oxides: potential impacts on drinking water quality. *Environ. Sci. Technol.* **2017**, *51* (12), 6812−6820.

(19) Cheng, F.; Su, Y.; Liang, J.; Tao, Z.; Chen, J. MnO_2-based nanostructures as catalysts for electrochemical oxygen reduction in alkaline media. *Chem. Mater.* **2010**, *22* (3), 898−905.

(20) Meng, Y.; Song, W.; Huang, H.; Ren, Z.; Chen, S. Y.; Suib, S. L. Structure−property relationship of bifunctional MnO_2 nanostructures: highly efficient, ultra-stable electrochemical water oxidation and oxygen reduction reaction catalysts identified in alkaline media. *J. Am. Chem. Soc.* **2014**, *136* (32), 11452−11464.

(21) Olesen, B. H.; Avci, R.; Lewandowski, Z. Manganese dioxide as a potential cathodic reactant in corrosion of stainless steels. *Corros. Sci.* **2000**, *42* (2), 211−227.

(22) McKenzie, R. M. The adsorption of lead and other heavy metals on oxides of manganese and iron. *Aust. J. Soil Res.* **1980**, *18*, 61−73.

(23) Dong, D.; Nelson, Y. M.; Lion, L. W.; Shuler, M. L.; Ghiorse, W. C. Adsorption of Pb and Cd onto metal oxides and organic material in natural surface coatings as determined by selective extractions: new evidence for the importance of Mn and Fe oxides. *Water Res.* **2000**, *34* (2), 427−436.

(24) Nelson, Y.; Lion, L.; Shuler, M.; Ghiorse, W. Lead binding to metal oxide and organic phases of natural aquatic biofilms. *Limnol. Oceanogr.* **1999**, *44* (7), 1715−1729.

(25) O'Reilly, S.; Hochella, M. J. Pb sorption efficiencies of natural and synthetic Mn and Fe-oxides. *Geochim. Cosmochim. Acta* **2003**, *67*, 4471−4487.

(26) Trueman, B. F.; Gagnon, G. A. A new analytical approach to understanding nanoscale lead-iron interactions in drinking water distribution systems. *J. Hazard. Mater.* **2016**, *311*, 151−157.

(27) Masters, S.; Edwards, M. Increased lead in water associated with iron corrosion. *Environ. Eng. Sci.* **2015**, *32* (5), 361−369.

(28) Pieper, K. J.; Tang, M.; Edwards, M. A. Flint water crisis caused by interrupted corrosion control: Investigating "ground zero" home. *Environ. Sci. Technol.* **2017**, *51* (4), 2007−2014.

(29) Friedman, M.; Hill, A.; Reiber, S.; Valentine, R. L.; Larsen, G.; Young, A.; Korshin, G. V.; Peng, C. Y. *Assessment of Inorganics Accumulation in Drinking Water System Scales and Sediments*; Water Research Foundation: Denver, CO, 2010.

(30) Nelson, Y.; Lion, L.; Ghiorse, W.; Shuler, M. Production of biogenic Mn oxides by Leptothrix discophora SS-1 in a chemically defined growth medium and evaluation of their Pb adsorption characteristics. *Appl. Environ. Microbiol.* **1999**, *65* (1), 175−180.

(31) Deutsch, W. J. *Groundwater geochemistry: Fundamentals and applications to contamination*; CRC Press: Boca Raton, FL, 1997; p 71.

(32) Hill, D. M.; Aplin, A. C. Role of colloids and fine particles in the transport of metals in rivers draining carbonate and silicate terrains. *Limnol. Oceanogr.* **2001**, *46* (2), 331−344.

(33) Gagnon, G.; Rand, J.; O'Leary, K.; Rygel, A.; Chauret, C.; Andrews, R. Disinfectant efficacy of chlorite and chlorine dioxide in drinking water biofilms. *Water Res.* **2005**, *39*, 1809−1917.

(34) Camper, A.; Brastrup, K.; Sandvig, A.; Clement, J.; Spencer, C.; Capuzzi, A. Effect of distribution system materials on bacterial regrowth. *J. - Am. Water Works Assoc.* **2003**, *95* (7), 107−121.

(35) Sharp, R.; Camper, A.; Crippen, J.; Schneider, J.; Leggiero, S. Evaluation of drinking water biostability using biofilm methods. *J. Environ. Eng.* **2001**, *127* (5), 403−411.

DOI: 10.1021/acs.est.9b00317
Environ. Sci. Technol. XXXX, XXX, XXX−XXX

(36) Fang, W.; Hu, J. Y.; Ong, S. L. Influence of phosphorus on biofilm formation in model drinking water distribution systems. *J. Appl. Microbiol.* **2009**, *106*, 1328−1335.
(37) Rygel, A. C. Manganese in drinking water distribution. PhD Dissertation, Dalhousie University, Halifax, Canada, 2006.
(38) Payne, S. J. Interactions of corrosion control and biofilm on lead and copper in premise plumbing. PhD Dissertation, Dalhousie University, Halifax, Canada, 2013.
(39) Wu, C. C.; Ghosh, S.; Martin, K. J.; Pinto, A. J.; Denef, V. J.; Olson, T. M.; Love, N. G. The microbial colonization of activated carbon block point-of-use (PoU) filters with and without chlorinated phenol disinfection by-products. *Environ. Sci. Water Res. Technol.* **2017**, *3* (5), 830−843.
(40) Rosario-Ortiz, F.; Rose, J.; Speight, V.; Von Gunten, U.; Schnoor, J. How do you like your tap water? *Science* **2016**, *351* (6276), 912−914.
(41) Schwake, D. O.; Garner, E.; Strom, O. R.; Pruden, A.; Edwards, M. A. Legionella DNA markers in tap water coincident with a spike in Legionnaires' disease in Flint, MI. *Environ. Sci. Technol. Lett.* **2016**, *3* (9), 311−315.
(42) Lytle, D. A.; Schock, M. R. Impact of stagnation time on metal dissolution from plumbing materials in drinking water. *Aqua* **2000**, *49* (5), 243−257.
(43) Trueman, B. F.; Krkošek, W. H.; Gagnon, G. A. Effects of ortho- and polyphosphates on lead speciation in drinking water. *Environ. Sci. Water Res. Technol.* **2018**, *4* (4), 505−512.
(44) Haas, C.; Koch, L.; Kelty, K.; Lytle, D.; Triantafyllidou, S. *Effectiveness of the preservation protocol within the Environmental Protection Agency (EPA) Method 200.8 for soluble and particulate lead recovery in drinking water*; US Environmental Protection Agency: Washington, DC, (EPA/600/R-13/222), 2013.
(45) Wang, Y.; Mehta, V.; Welter, G. J.; Giammar, D. E. Effect of connection methods on lead release from galvanic corrosion. *J. - Am. Water Works Assoc.* **2013**, *105* (7), E337−E351.
(46) Wang, Y.; Jing, H.; Mehta, V.; Welter, G. J.; Giammar, D. E. Impact of galvanic corrosion on lead release from aged lead service lines. *Water Res.* **2012**, *46* (16), 5049−5060.
(47) American Public Health Association *American Waterworks Association, Water Pollution Control Federation. Standard Methods For the Examination of Water and Wastewater*, 22nd ed.; American Public Heath Association: Washington, DC, 2012.
(48) Rollie, M. E.; Patonay, G.; Warner, I. M. Deoxygenation of solutions and its analytical applications. *Ind. Eng. Chem. Res.* **1987**, *26* (1), 1−6.
(49) Revie, R. W., Uhlig, H. H. *Corrosion and corrosion control: an introduction to corrosion science and engineering*; John Wiley & Sons: Hoboken, NJ, 2008.
(50) Biswal, A.; Tripathy, B. C.; Sanjay, K.; Subbaiah, T.; Minakshi, M. Electrolytic manganese dioxide (EMD): a perspective on worldwide production, reserves and its role in electrochemistry. *RSC Adv.* **2015**, *5* (72), 58255−58283.
(51) Mirza, A.; Burr, M.; Ellis, T.; Evans, D.; Kakengela, D.; Webb, L.; Gagnon, J.; Leclercq, F.; Johnston, A. Corrosion of lead anodes in base metals electrowinning. *J. South. Afr. Inst. Min. Metall.* **2016**, *116* (6), 533−538.
(52) Shi, Z.; Stone, A. T. PbO_2 (s, plattnerite) reductive dissolution by aqueous manganous and ferrous ions. *Environ. Sci. Technol.* **2009**, *43* (10), 3596−3603.
(53) Allward, N. E.; Gregory, B. S.; Sotddart, A. K.; Gagnon, G. A. Potential for manganese biofouling in water transmission lines using model reactors. *Environ. Sci.: Water Res. Technol.* **2018**, *4*, 761−772.
(54) Itoh, A.; Kimata, C.; Miwa, H.; Sawatari, H.; Haraguchi, H. Speciation of trace metals in pond water as studied by liquid chromatography/inductively coupled plasma mass spectrometry. *Bull. Chem. Soc. Jpn.* **1996**, *69* (12), 3469−3473.
(55) Kozai, N.; Ohnuki, T.; Iwatsuki, T. Characterization of saline groundwater at Horonobe, Hokkaido, Japan by SEC-UV-ICP-MS: Speciation of uranium and iodine. *Water Res.* **2013**, *47* (4), 1570−1584.
(56) Lyvén, B.; Hassellöv, M.; Turner, D. R.; Haraldsson, C.; Andersson, K. Competition between iron-and carbon-based colloidal carriers for trace metals in a freshwater assessed using flow field-flow fractionation coupled to ICPMS. *Geochim. Cosmochim. Acta* **2003**, *67* (20), 3791−3802.
(57) Zhang, Y.; Chen, Y.; Westerhoff, P.; Crittenden, J. Impact of natural organic matter and divalent cations on the stability of aqueous nanoparticles. *Water Res.* **2009**, *43*, 4249−4257.
(58) Sander, S.; Mosley, L. M.; Hunter, K. A. Investigation of interparticle forces in natural waters: Effects of adsorbed humic acids on iron oxide and alumina surface properties. *Environ. Sci. Technol.* **2004**, *38*, 4791−4796.
(59) Chekli, L.; Phuntsho, S.; Roy, M.; Shon, H. K. Characterisation of Fe-oxide nanoparticles coated with humic acid and Suwannee River natural organic matter. *Sci. Total Environ.* **2013**, *461−462*, 19−27.
(60) Chin, Y. P.; Aiken, G.; O'Loughlin, E. Molecular weight, polydispersity, and spectroscopic properties of aquatic humic substances. *Environ. Sci. Technol.* **1994**, *28* (11), 1853−1858.
(61) Rahman, M. S.; Whalen, M.; Gagnon, G. A. Adsorption of dissolved organic matter (DOM) onto the synthetic iron pipe corrosion scales (goethite and magnetite): Effect of pH. *Chem. Eng. J.* **2013**, *234*, 149−157.
(62) Spencer, R. G.; Butler, K. D.; Aiken, G. R. Dissolved organic carbon and chromophoric dissolved organic matter properties of rivers in the USA. *J. Geophys. Res. Biogeosci.* **2012**, *117*, G03001.
(63) Vogl, J.; Heumann, K. G. Determination of heavy metal complexes with humic substances by HPLC/ICP-MS coupling using on-line isotope dilution technique. *Fresenius' J. Anal. Chem.* **1997**, *359* (4−5), 438−441.
(64) Schock, M. R.; Lytle, D. A.; Sandvig, A. M.; Clement, J.; Harmon, S. M. Replacing polyphosphate with silicate to solve lead, copper, and source water iron problems. *J. - Am. Water Works Assoc.* **2005**, *97* (11), 84−93.
(65) Edwards, M.; McNeill, L. S. Effect of phosphate inhibitors on lead release from pipes. *J. - Am. Water Works Assoc.* **2002**, *94* (1), 79−90.
(66) Zhao, J.; Giammar, D. E.; Pasteris, J. D.; Dai, C.; Bae, Y.; Hu, Y. Formation and aggregation of lead phosphate particles: Implications for lead immobilization in water supply systems. *Environ. Sci. Technol.* **2018**, *52* (21), 12612−12623.
(67) Schock, M. R.; Wagner, I.; Oliphant, R. J. Corrosion and Solubility of Lead in Drinking Water. In *Internal Corrosion of Water Distribution Systems*; AWWA Research Foundation: Denver, CO, 1996; pp 131−230.
(68) Lytle, D. A.; Schock, M. R.; Scheckel, K. The inhibition of Pb (IV) oxide formation in chlorinated water by orthophosphate. *Environ. Sci. Technol.* **2009**, *43* (17), 6624−6631.
(69) Cerrato, J. M.; Falkinham, J. O., III; Dietrich, A. M.; Knocke, W. R.; McKinney, C. W.; Pruden, A. Manganese-oxidizing and-reducing microorganisms isolated from biofilms in chlorinated drinking water systems. *Water Res.* **2010**, *44* (13), 3935−3945.
(70) Cuss, C. W.; Grant-Weaver, I.; Shotyk, W. AF4-ICPMS with the 300 Da membrane to resolve metal-bearing "colloids"< 1 kDa: optimization, fractogram deconvolution, and advanced quality control. *Anal. Chem.* **2017**, *89* (15), 8027−8035.
(71) Katsoyiannis, I. A.; Zouboulis, A. I. Biological treatment of Mn (II) and Fe (II) containing groundwater: kinetic considerations and product characterization. *Water Res.* **2004**, *38* (7), 1922−1932.
(72) Cerrato, J. M.; Hochella, M. F., Jr; Knocke, W. R.; Dietrich, A. M.; Cromer, T. F. Use of XPS to identify the oxidation state of Mn in solid surfaces of filtration media oxide samples from drinking water treatment plants. *Environ. Sci. Technol.* **2010**, *44* (15), 5881−5886.
(73) Galakhov, V. R.; Uhlenbrock, S.; Bartkowski, S.; Postnikov, A. V.; Neumann, M.; Finkelstein, L. D.; Kurmaev, E. Z.; Samokhvalov, A. A.; Leonyuk, L. I. X-ray photoelectron 3s spectra of transition metal oxides. 1999. arXiv:cond-mat/9903354 [cond-mat.mtrl-sci].
(74) Taffarel, S. R.; Rubio, J. Removal of Mn^{2+} from aqueous solution by manganese oxide coated zeolite. *Miner. Eng.* **2010**, *23* (14), 1131−1138.

DOI: 10.1021/acs.est.9b00317
Environ. Sci. Technol. XXXX, XXX, XXX−XXX

(75) Cardinale, B. J.; Matulich, K. L.; Hooper, D. U.; Byrnes, J. E.; Duffy, E.; Gamfeldt, L.; Balvanera, P.; O'Connor, M. I.; Gonzalez, A. The functional role of producer diversity in ecosystems. *Am. J. Bot.* **2011**, *98*, 572−592.
(76) Tilman, D.; Harpole, W. S. Grassland species loss resulting from niche dimension. *Nature* **2007**, *446*, 791−793.
(77) Wang, J.; Pan, F.; Soininen, J.; Heino, J.; Shen, J. Nutrient enrichment modifies temperature-biodiversity relationships in large-scale field experiments. *Nat. Commun.* **2016**, *7*, 13960.
(78) Mouchet, P. From conventional to biological removal of iron and manganese in France. *J. - Am. Water Works Assoc.* **1992**, *84*, 158−167.
(79) Gregory, E.; Staley, J. T. Widespread distribution of ability to oxidize manganese among freshwater bacteria. *Appl. Environ. Microbiol.* **1982**, *44*, 509−511.
(80) Akob, D.; Bohu, T.; Beyer, A.; Schaffner, F.; Handel, M.; Johnson, C.; Merten, D.; Buchel, G.; Totsche, U.; Kusel, K. Identification of Mn(II)-oxidizing bacteria from a low-pH contaminated former uranium mine. *Appl. Environ. Microbiol.* **2014**, *80*, 5086−5097.
(81) Hansel, C.; Francis, C. Coupled photochemical and enzymatic Mn(II) oxidation pathways of a planktonic *Roseobacter*-like bacterium. *Appl. Environ. Microbiol.* **2006**, *72* (5), 3543−3549.
(82) White, C.; Tancos, M.; Lytle, D. A. Microbial community profile of a lead service line removed from a drinking water distribution system. *Appl. Environ. Microbiol.* **2011**, *77* (15), 5557−5561.
(83) Borremans, B.; Hobman, J.; Provoost, A.; Brown, N.; van Der Leslie, D. Cloning and functional analysis of the pbr lead resistance determinant of *Ralstonia metallidurans* CH34. *J. Bacteriol.* **2001**, *183* (19), 5651−8.
(84) Wang, X.; Chen, M.; Xiao, J.; Hao, L.; Crowley, D.; Zhang, Z.; Yu, J.; Huang, N.; Huo, M.; Wu, J. Genome sequence analysis of the naphthenic acid degrading and metal resistance bacterium *Cupriavidus gilardii* CR3. *PLoS One* **2015**, *10* (8), No. e0132881.
(85) Mergeay, M.; Nies, D.; Schlegel, H.; Gerits, J.; Charles, P.; Van Gijsegem, F. *Alcaligenes eutrophus* CH34 is a facultative chemolithotroph with plasmid-bound resistance to heavy metals. *J. Bacteriol.* **1985**, *162* (1), 328−34.
(86) Kehres, D.; Zaharik, M.; Finlay, B.; Maguire, M. The NRAMP proteins of *Salmonella typhimurium* and *Escherichia coli* are selective manganese transporters involved in the response to reactive oxygen. *Mol. Microbiol.* **2000**, *36* (5), 1085−1100.
(87) Payne, S.; Piorkowski, G.; Hansen, L.; Gagnon, G. Impact of zinc orthophosphate on simulated drinking water biofilms influenced by lead and copper. *J. Environ. Eng.* **2016**, *142* (2), 04015067.
(88) An, F.; Zhan, D. Microbial diversity and community structure in agricultural soils suffering from 4-year Pb contamination. *Can. J. Microbiol.* **2018**, *64* (5), 305−316.
(89) Drewniak, L.; Krawczyk, P.; Mielnicki, S.; Adamska, D.; Sobczak, A.; Lipinski, L.; Burec-Drewniak, W.; Sklodowska, A. Physiological and metagenomic analyses of microbial mats involved in self-purification of mine waters contaminated with heavy metals. *Front. Microbiol.* **2016**, *7*, 1252.
(90) Golby, S.; Ceri, H.; Marques, L.; Turner, R. Mixed-species biofilms cultured from an oil sand tailings pond can biomineralize metals. *Microb. Ecol.* **2014**, *68*, 70−80.
(91) Bowman, N.; Patel, D.; Sanchez, A.; Xu, W.; Alsaffar, A.; Tiquia-Arashiro, S. Lead-resistant bacteria from Saint Clair River sediments and Pb removal in aqueous solutions. *Appl. Microbiol. Biotechnol.* **2018**, *102*, 2391−2398.
(92) Li, J.; Peng, X.; Zhou, H.; Li, J.; Sun, Z. Molecular evidence for microorganisms participating in Fe, Mn, and S biogeochemical cycling in two low-temperature hydrothermal fields at the Southwest Indian Ridge. *J. Geophys. Res.: Biogeosci.* **2013**, *118*, 665−679.
(93) Korshin, G. V.; Ferguson, J. F.; Lancaster, A. N.; Wu, H. *Corrosion and Metal Release for Lead-Containing Materials: Influence of NOM*; AWWA Research Foundation: U.S.A., 1999.
(94) Gao, Y.; Trueman, B. F.; Stoddart, A. K.; Gagnon, G. A. Understanding the impact of extracellular polymeric substances on lead release in drinking water systems. *ACS Omega* **2018**, *3* (11), 14824−14832.
(95) Arnold, R. B., Jr; Edwards, M. Potential reversal and the effects of flow pattern on galvanic corrosion of lead. *Environ. Sci. Technol.* **2012**, *46* (20), 10941−10947.

DOI: 10.1021/acs.est.9b00317
Environ. Sci. Technol. XXXX, XXX, XXX−XXX